



ELSEVIER

Journal of Volcanology and Geothermal Research 62 (1994) 137-151

Journal of volcanology and
geothermal research

Earthquake classification, location, and error analysis in a volcanic environment: implications for the magmatic system of the 1989-1990 eruptions at Redoubt Volcano, Alaska

J.C. Lahr, B.A. Chouet, C.D. Stephens, J.A. Power, R.A. Page

au.s. Geological Survey, 345 Middlefield Road, MS 977, Menlo Park, CA 94025, USA
bU.S. Geological Survey, Geophysical Institute, University of Alaska, Fairbanks, AK 99775, USA

Received 17 April 1992; revised version accepted 20 September 1993

Abstract

Determination of the precise locations of seismic events associated with the 1989-1990 eruptions of Redoubt Volcano posed a number of problems, including poorly known crustal velocities, a sparse station distribution, and an abundance of events with emergent phase onsets. In addition, the high relief of the volcano could not be incorporated into the HYPOELLIPSE earthquake location algorithm. This algorithm was modified to allow hypocenters to be located above the elevation of the seismic stations. The velocity model was calibrated on the basis of a post-eruptive seismic survey, in which four chemical explosions were recorded by eight stations of the permanent network supplemented with 20 temporary seismographs deployed on and around the volcanic edifice. The model consists of a stack of homogeneous horizontal layers; setting the top of the model at the summit allows events to be located anywhere within the volcanic edifice. Detailed analysis of hypocentral errors shows that the long-period (LP) events constituting the vigorous 23-hour swarm that preceded the initial eruption on December 14 could have originated from a point 1.4 km below the crater floor. A similar analysis of LP events in the swarm preceding the major eruption on January 2 shows they also could have originated from a point, the location of which is shifted 0.8 km northwest and 0.7 km deeper than the source of the initial swarm. We suggest this shift in LP activity reflects a northward jump in the pathway for magmatic gases caused by the sealing of the initial pathway by magma extrusion during the last half of December. Volcano-tectonic (VT) earthquakes did not occur until after the initial 23-hour-long swarm. They began slowly just below the LP source and their rate of occurrence increased after the eruption of 01:52 AST on December 15, when they shifted to depths of 6 to 10 km. After January 2 the VT activity migrated gradually northward; this migration suggests northward propagating withdrawal of magma from a plexus of dikes and/or sills located in the 6 to 10 km depth range. Precise relocations of selected events prior to January 2 clearly resolve a narrow, steeply dipping, pencil-shaped concentration of activity in the depth range of 1-7 km, which illuminates the conduit along which magma was transported to the surface. A third event type, named hybrid, which blends the characteristics of both VT and LP events, originates just below the LP source, and may reflect brittle failure along a zone intersecting a fluid-filled crack. The distribution of hybrid events is elongated 0.2-0.4 km in an east-west direction. This distribution may offer constraints on the orientation and size of the fluid-filled crack inferred to be the source of the LP events.

1. Introduction

The first unequivocal sign of reawakening of Redoubt Volcano in December 1989 after 23 years of quiescence was an energetic swarm of seismicity made up exclusively of long-period (LP) events commonly associated with magmatic activity (Koyanagi et al., 1987). Volcano-tectonic (VT) earthquakes began to occur at shallow depths soon after the first eruption, and within one day shifted to the 5-10 km depth range. Power et al. (1994-this volume) describe the evolution of the seismic activity and eruptions. Chouet et al. (1994-this volume) describe the use of LP swarms as precursory indicators of tephra eruptions and develop a physical model for the generation of long-period events. Stephens et al. (1994-this volume) interpret the seismic spectral data which were recorded in real time throughout the eruptive sequence. This paper details the methods used and problems encountered in classifying and locating the seismic activity, estimates the hypocentral precision and accuracy for the different types of seismic events, interprets the spatial relationships among event types, and discusses the magnitude distribution of the seismicity, with particular emphasis on the LP swarm leading to the first eruption.

2. Seismic network

At the onset of the eruption of Redoubt Volcano in December 1989 five stations were operating in the vicinity of the volcano (see Fig. 1), although DFR worked only intermittently until January 2, 1990. RDN's operation was impaired by the eruptions of December 14, but data from this station continued to be useful for determining P-phase arrival times until the radio transmitter was damaged by electrostatic discharge associated with the pyroclastic flows of January 2. The station was repaired on January 9 but was permanently disabled by another pyroclastic flow on February 15. During February and March four additional stations were installed, three of which

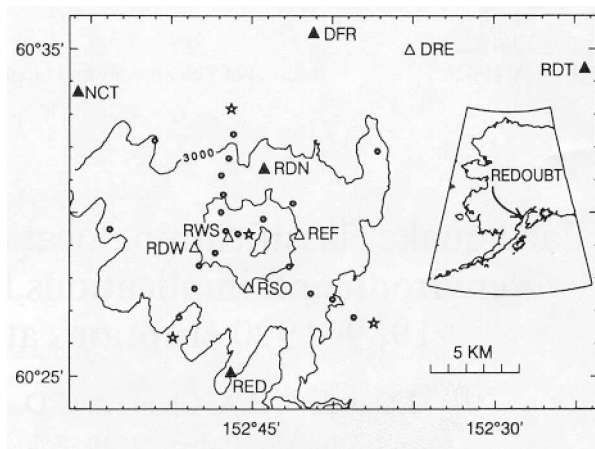


Fig. 1. Map of Redoubt Volcano area showing original seismic stations (solid triangles), subsequent additional stations (open triangles), temporary digital seismographs (circles), and shot points (stars). RDT and the digital stations monitor three components of motion while the remaining stations each have a single-component vertical geophone. Elevation contours with 3000-ft interval are shown for Redoubt. Inset map shows location of Redoubt Volcano within Alaska.

were located on the volcanic edifice (Fig. 1). See Power et al. (1994-this volume) for details of network operation. The three stations on the edifice proved critical to monitoring the volcano during the waning phase of the eruption sequence, as the events associated with premonitory LP swarms generally became too small to be detected on more distant stations (Stephens et al., 1994-this volume). This paper focuses on the events recorded during the interval December 1989-January 1990, the vast majority of which were located with a P-phase arrival at RDN and both P- and S-phase arrivals at RED, NCT, and RDT. Each station included a I-Hz vertical-component L-4C geophone, the signal from which was telemetered in analog format to Fairbanks, Alaska, and then digitized by a 12-bit A/D converter at 100.2 Hz and recorded on a PC computer running the MDETECT data acquisition program (Tottingham et al., 1988). The displacement sensitivity of a typical station peaks near 15 Hz and is about 75 digital counts per millimicron at this frequency. Local magnitudes

were computed by the program HYPOELLIPSE (Lahr, 1989) from measurements of the maximum trace amplitude and corresponding period of the vertical component.

From July 3 to 26, 1991, 20 Reftek digital seismic recorders, loaned by IRIS-PASSCAL, were temporarily installed on and around Redoubt Volcano to augment the permanent stations (Fig. 1). Each temporary station recorded a 2-Hz, 3-component L-22 sensor on a hard disk. The sampling rate for preassigned shot windows and triggered events was 100 Hz, while the vertical component was recorded continuously at 50 Hz. The recorders were deployed for about 3 weeks, during which we recorded four chemical explosions (Fig. 1), thousands of natural events (most originating from the upper 8 km beneath Redoubt Volcano), several hundred earthquakes from the Wadati-Benioff zone which underlies the volcanic axis, and a few teleseisms. In this paper a preliminary analysis of the shot recordings is used to help constrain a velocity model consisting of homogeneous horizontal layers. Inversion of these data to determine the three-dimensional velocity structure of the volcano is now in progress (Dawson et al., 1992).

3. Event classification

The goal of event classification at Redoubt Volcano was to separate events recorded by the local seismograph network into categories according to the source process involved, rather than simply on the basis of waveform similarities [see also Chouet et al. (1994-this volume) and Power et al. (1994-this volume)]. When correctly done, this classification provides greater insight into the different types of physical processes associated with volcanic activity. The entire data set was initially classified on the basis of the time-domain appearance of the seismograms as viewed on a computer screen. Although this method provided a good preliminary classification, the data for the interval December 1, 1989-January 2, 1990 were reviewed again with the aid of spectral analyses. In one type of representation a 40.6-s seismogram was divided into

a series of 1.27-s windows, each offset 0.63 s from the previous window. The spectral amplitudes of the vertical component of ground velocity were computed for each window and contoured for the frequency range 0-15 Hz and time range 0-40.6 s (Figs. 2a, 2c, 3a, and 3c). These contour plots, or spectrograms, are normalized to a peak value of 15 counts, with contours every unit and bold contours every 5 units. Such spectrograms are useful in appraising the spectral content of the

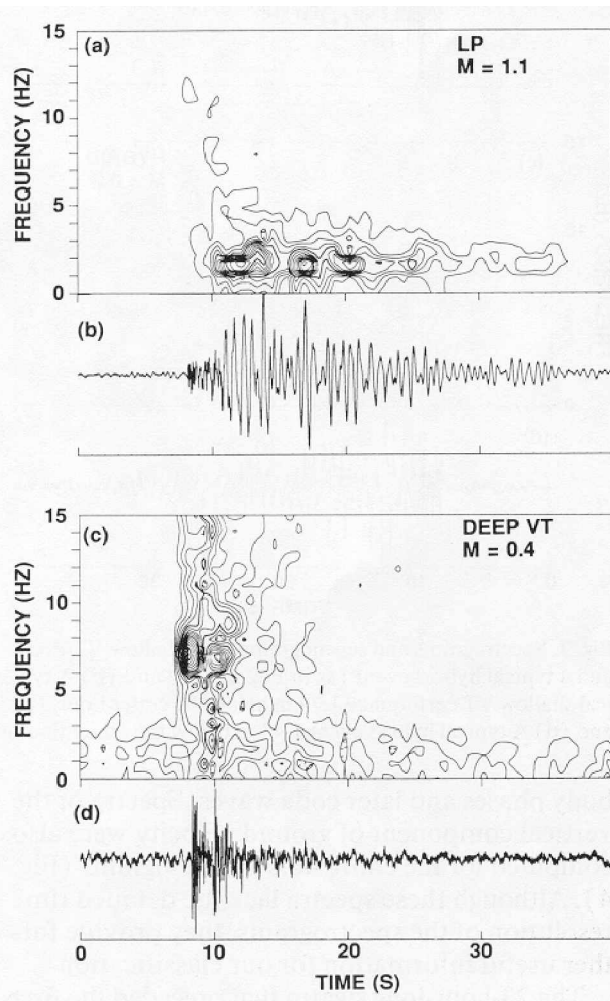


Fig. 2. Spectrograms and seismograms for a typical LP event and a deep VT event. Amplitude spectral density of vertical component of ground velocity at RED versus time (a) and seismogram (b) for a typical long-period event of the December 13-14 swarm centered 1.4 km below the crater floor. (c) and (d) Corresponding plots for a typical VT earthquake 8.4 km below the crater floor.

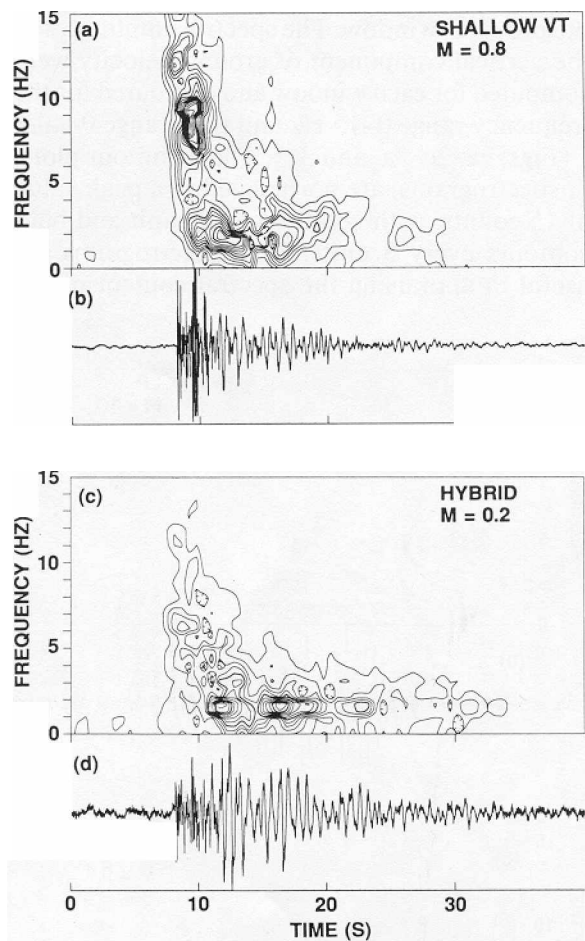


Fig. 3. Spectrograms and seismograms for a shallow VT event and a typical hybrid event (as in Fig. 2). (a) and (b) A typical shallow VT earthquake 1.7 km below the crater floor. (c) and (d) A typical hybrid event 1.4 km below the crater floor.

body phases and later coda waves. Spectra of the vertical component of ground velocity were also computed for the entire 40.6-s seismograms (Fig. 4). Although these spectra lack the detailed time resolution of the spectrograms, they provide further useful information for our classification.

The 23-hour-long swarm that preceded the first eruption on December 13 consisted exclusively of long-period events (Stephens et al., 1994-this volume). The events of this swarm were characterized at RED by a weak high-frequency onset with frequencies up to 10 Hz, followed about 2 seconds later by strong, quasi-monochromatic

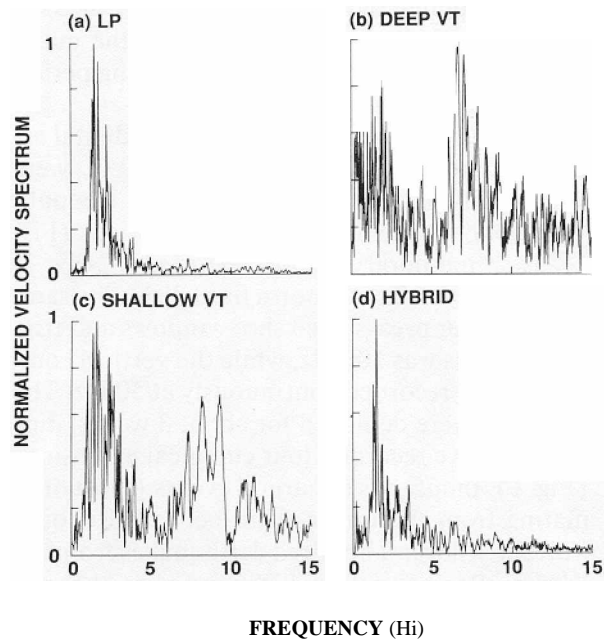


Fig. 4. Normalized velocity spectra of the typical LP, deep VT, shallow VT, and hybrid events shown in Figs. 2 and 3. Each seismogram was 40.6 s in duration and included 4096 digital samples.

oscillations with a peak frequency near 1.5 Hz and lasting 20 seconds or more (Fig. 2b). Energy in the band of 1.2-2.5 Hz dominates both the spectrum (Fig. 4a) and the spectrogram (Fig. 2a). The LP events are attributed to the resonance of fluid-filled cracks or conduits induced by pressure transients in the fluid (Aki et al., 1977; Chouet, 1985, 1988, 1992). Whenever clear, the first motions from events in this LP swarm were all dilatations.

Typical short-period earthquakes, termed volcano-tectonic earthquakes when they occur within or under a volcanic edifice, are attributed to brittle failure in response to stress changes associated with magmatic activity. For sources below a few kilometers depth, VT earthquakes have clear high-frequency P and S arrivals with peak frequencies above 5 Hz and are easily distinguished from LP events. The seismogram of a typical deep VT earthquake is dominated by the P- and S phases and a very short coda (Fig. 2d). The spectrogram shows broadband P- and S phases with peak energy between 6 and 8 Hz, and

has a broadband coda with energy extending up to 15 Hz (Fig. 2c). Shallow VT quakes larger than about M 0.3 generated stronger surface waves than the deeper VT earthquakes (compare Figs. 2d and 3b) but were still distinguishable from LP events on recordings obtained at RED. Notice the variation in dominant coda frequency with time in the seismogram and spectrogram of a typical shallow VT, from 1.5 Hz three seconds after the S phase to 3 Hz five seconds later (Figs. 3a and 3b); such variation is characteristic of a dispersed surface wave train. Shallow VT's smaller than about M 0.3 that occur within the coda of LP events can not be easily distinguished from the latter, so that some of the smallest events located may be misclassified.

All of the events were originally classified on the basis of their seismograms as either LP or VT. However, questions remained as to the correct classification for some of the shallow events that occurred between December 15 and January 3. To address this question, (40.6-s seismogram and its spectrum were plotted for all the triggered events during this time interval. Inspection of these plots indicated that a third type of event with mixed characteristics, called a hybrid event, was common during this time interval. Hybrid events have more pronounced high-frequency onsets than LP events (compare Figs. 2b and 3d) and show a mix of first motions characteristic of VT earthquakes. Their codas, however, are dominated by a non-dispersive harmonic wave train that is characteristic of LP events, hence the spectrograms of a hybrid coda and an LP coda are similar (compare Figs. 3c and 2a). We suggest that the hybrid events may result from brittle faulting in zones of weakness intersecting a fluid-filled crack and thus involve both double-couple and volumetric source components.

4. Location procedures

To account for different station elevations, standard earthquake location algorithms incorporate any delay due to station elevation differences into the station correction, as in HYPO71

(Lee and Lahr, 1975) and HYPOINVERSE (Klein, 1978), or use the elevation of the station above sea level to compute a separate elevation correction, as in HYPOELLIPSE (Lahr, 1989). Inherent in these approaches is the assumption that the earthquake sources are located below the elevation of the lowest station. On a stratovolcano, however, this assumption is often not valid. In the case of Redoubt Volcano, for example, seismic events were located as shallow as the crater floor at an elevation of 2.3 km above sea level, whereas station elevations ranged from 0.5 to 2.7 km above sea level. To address this problem, the travel time algorithm in HYPOELLIPSE was modified in a manner similar to the algorithm used in HYPOCENTER (Lienert et al., 1986; B.R. Lienert, pers. commun., 1991). In this modified code, the elevation of the top of the flat-layered velocity model may be specified to match the elevation of the highest relief in the region under study. Stations at lower elevations are imbedded within the model, and may be located within any layer. Travel times and take-off angles are computed for the true relative locations of source and station.

For the present study, the top of the model was fixed at 3 km above sea level, nearly coincident with the elevation of the summit of Redoubt Volcano (Fig. 5). However, we found no evidence of any events occurring above the elevation of the crater floor. For this reason, depths are referred to the 2.3 km elevation of the crater floor in all the hypocenter plots shown in this paper. Negative depths of up to -0.7 km only reflect the poor depth constraint of some of the data.

5. Velocity model

During the July 1991 experiment the 8-station permanent network was supplemented by 20 digital Reftek seismographs (Fig. 1). Four 450-kg chemical charges were detonated, one in a glacial crevasse in the summit crater 200 m east of the lava dome and three in meltwater kettles in the piedmont lobes of glaciers at the base of the volcano.

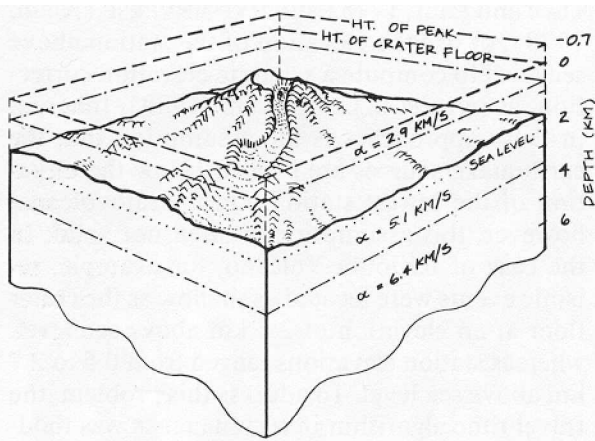


Fig. 5. Sketch of Redoubt Volcano viewed from the north-west illustrating the relationship between the flat-layered velocity model used in computing earthquake locations and the topography of the volcano. Compressional velocities, a , are shown. All depths are referenced to the height of the crater floor, 2.3 km above sea level. The first layer of the model extends from the peak of the volcano, about 0.7 km above the crater floor, to 0.6 km below the crater floor. The second layer continues to 3.8 km depth, while the third extends to at least 19 km depth. Note that the location program will allow solutions anywhere within the velocity model, including above the surface of the earth, the latter being artifacts due to location errors.

Data from these four shots helped constrain the flat-layered velocity model used in this study. Special emphasis was placed on matching the observed and computed travel times from the crater Shot, which was located directly above the shallow precursory seismicity. The P arrivals from these explosions are compatible with a compressional velocity a of 2.9 km/s in a layer extending to a depth of 0.6 km below the crater floor and overlaying a 3.2-km-thick layer with $\alpha=5.1$ km/s (Fig. 5). P- and S-arrivals from LP events were found to be most consistent with a compressional-to-shear wave velocity ratio (α/β) of 1.8 for these first two layers. A P velocity of $\alpha=6.4$ km/s and $\alpha/\beta=1.72$ were selected for the next layer to minimize the root-mean-square travel time residuals for well recorded VT earthquakes in the 5-10 km depth range. No rays penetrated below the 6.4 km/s layer, hence the thickness of this layer was not constrained.

Using this velocity model the errors in the

location for the summit shot determined from p phases from both 6 permanent and 18 temporary stations were 30 m for epicenter and 70 m for depth. The accuracy of the flank shot locations was poorer: epicentral errors of 400 to 1,750 m and depth errors of 660 to 1,540 m. Only six permanent stations (REF, RSO, RDW, RDN, DFR, and NCT) recorded the crater shot. The location of the crater shot based on only these p arrivals was in error by 40 m in epicenter and 90 m in depth. RDT and RED did not record the crater shot, so a direct estimate cannot be made of location bias of events that occurred prior to January 2, 1990, when only RDT, RED, RDN, NCT, and DFR were available. We estimate that the epicentral bias was less than 150 m for the shallow seismicity beneath the dome before RDN failed on January 2. This maximum bias was somewhat reduced after March 19 when stations RWS, RSO, and REF were all operating within 3.5 km of the crater.

6. LP event locations

The locations of LP events during the initial swarm of December 13-14 define a vertical cylindrical region extending from the crater floor to a depth of 3 km, with approximate north-south and east-west dimensions of 0.7 and 1.4 km, respectively. This distribution, which is appealing in terms of possibly defining a vertical conduit, cannot be reconciled with the observation that the waveforms and spectra of the events are all nearly identical (Chouet et al., 1994-this volume). In fact, when the events are subdivided into groups by magnitude range the scatter in the locations is observed to increase with decreasing magnitude (Fig. 6). This observation suggests that the overall distribution of hypocenters is an artifact caused by progressively greater difficulties in correctly picking the phase onsets of events of decreasing magnitude. Not only are the reading errors larger for the smaller events, but fewer phases can be picked at all.

To determine the size of the reading errors as a function of magnitude, we first assumed that all of the events occurred at a fixed location given

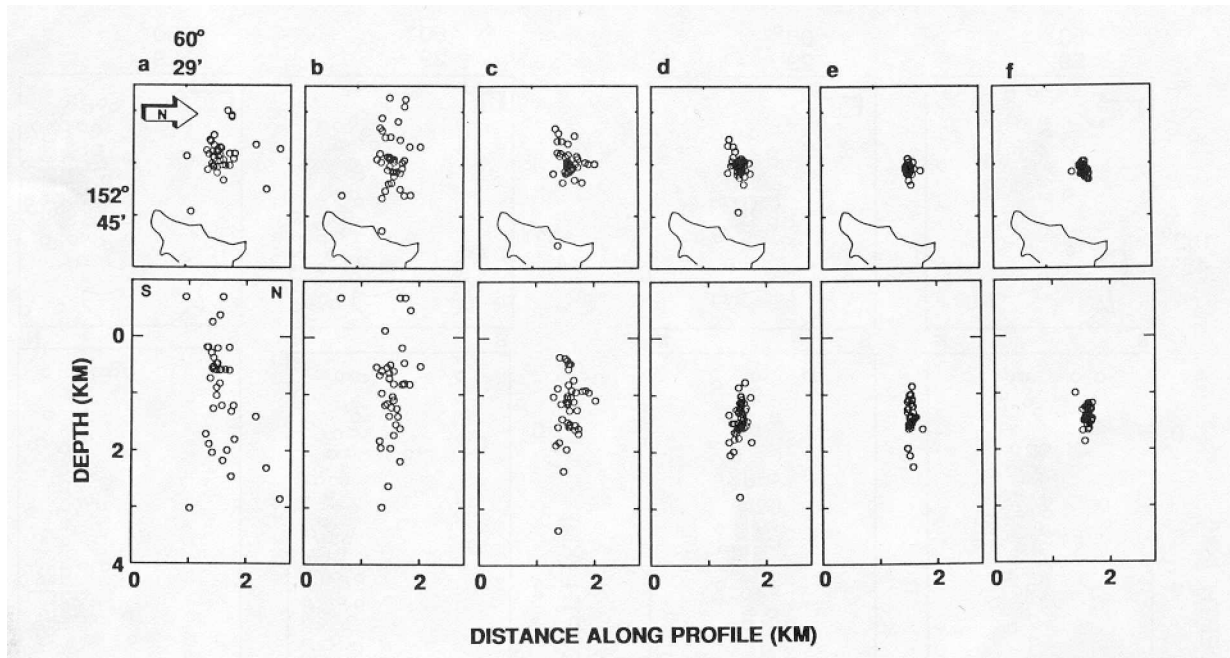


Fig. 6. Maps and north-south vertical sections of the LP event swarm of December 13-14 for different magnitude classes: (a) $MO.4-0.5$, (b) $MO.6-0.7$, (c) $MO.8-1.0$, (d) $M 1.1-1.2$, (e) $M 1.3$, and (f) $M 1.4-1.6$. The number of events in the various magnitude classes ranges from 40 to 58. The maps are rotated 90° clockwise; north is to the right and the scale is the same in both the maps and the cross sections. The 9000-ft summit elevation contour is shown for reference (see Fig. 1).

by the average location of events with magnitudes larger than 1.3. Then, keeping the hypo-centers fixed at the average location but allowing the origin times to vary, we computed the residuals between the observed and calculated arrival times. The standard deviations of the residuals for both P- and S phases were determined for all six magnitude intervals. We used these values to establish a relationship between standard deviation (SD) and magnitude (M):

$$SD = a + b \exp(-cM)$$

For the P phases the parameters a , b , and c are 0.005, 0.165, and 1.87, respectively. We found the standard deviation for S phases to be 1.7 times larger than that for P phases.

To demonstrate that random errors of this size can account for the observed scatter of the LP events, we perturbed the exact travel times for a postulated event fixed at the best location (cross in Fig. 7) with random errors modeling the observed standard deviations. A set of synthetic events was thus created in which the number of

events, the phases used, and the magnitudes corresponded to the actual data, but the arrival times corresponded to those of the postulated LP event plus a random error. The error was randomly selected from a Gaussian distribution with a mean of zero and standard deviation given by the above expression evaluated for the magnitude of the event. The distribution of locations for the real data is well replicated by that of the synthetic data, both in overall depth range and in the tendency for the east-west scatter to be greater than the north-south scatter (compare left and right Fig. 7).

Using the same relationship between standard deviation and magnitude, we similarly investigated the LP swarm of December 26-January 2, with the result that the synthetic data again replicate the real data (compare left and right Fig. 8). Note, however, that the locations in this later swarm are more scattered than in the earlier one. There are two reasons for this. First, the magnitudes were smaller than those in the first swarm, and the generally poorer signal-to-noise ratio,

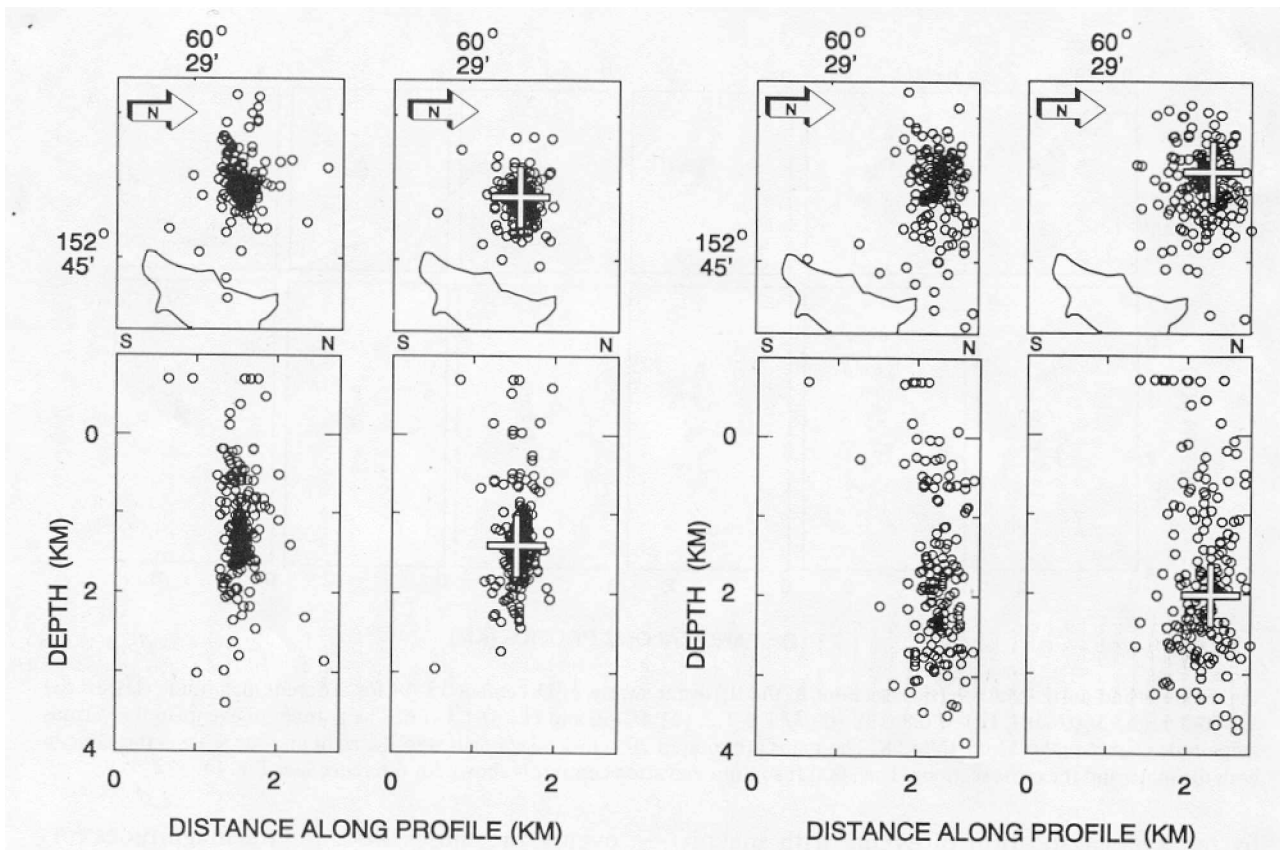


Fig. 7. Comparison of calculated (left) and synthetic (right) hypocenters of the initial LP swarm of December 13-14. Up- per: map view, rotated so that north is to the right. Lower: north-south vertical section. Synthetic data are perturbations of the postulated true location (cross) produced by incorporating variations in the phases used and random reading errors as described in text. Cross positioned at average location of events with magnitudes larger than 1.3.

coupled with the effects of medium heterogeneity, cause the phase arrivals to be more emergent. Second, the closest station (RDN) was damaged during the first eruption: its geophone resonated, initially at about 3 Hz and later near 5 Hz (Stephens et al., 1994-this volume). This resonance made unambiguous recognition of the onsets of the P arrivals at RDN difficult.

Given the uncertainty in the arrival times, neither of these clusters of LP events can be distinguished from a point source. Considering our ability to locate the crater shot with an accuracy of better than 100 m, and given the close proximity of the LP sources to the crater shot, we

Fig. 8. Comparison of calculated (left) and synthetic (right) hypocenters of the LP swarm of December 26-January I as in Fig. 7. Cross indicates location of postulated true location.

estimate the accuracy of these LP point sources to be better than 150 m horizontally and 500 m vertically.

In view of the source model of long-period events proposed by Chouet et al. (1994-this volume), the shift in the location of the LP source by 0.8 km to the northwest and 0.7 km deeper between December 14 and 27 may be interpreted to represent a shift in the gas flow to a more northerly pathway. An alternate explanation, which would also explain the change in arrival time pattern, would be a change in seismic velocity along the wave-propagation path to RED between December 14 and 27 that would increase the travel time to this station. This explanation is precluded by the occurrence on December 17 and 18 of a few LP events showing both the initial and latter arrival time patterns.

7. VT earthquake locations

We investigated the scatter in the distribution of volcano-tectonic earthquakes resulting from phase-picking errors by carefully analyzing the arrivals of 57 earthquakes, including 23 earthquakes from December 15-16 when most were shallower than 3 km depth, and 34 earthquakes from December 27 when most were deeper than 3 km. For each earthquake a record section was plotted showing the RDN, NCT, RED, and RDT traces with a time resolution of 0.01 s. Using a light table to overlay and compare events, we found 36 earthquakes belonged to one of 10 families defined by nearly identical waveforms and arrival times. By comparing earthquakes within each family, we were able to uniformly pick P phases at all four stations and S phases at all stations but RDN. As mentioned earlier the RDN response was anomalous much of the time, preventing reliable identification of the S phase at this station. With the exception of a small number of cases, in most of which the seismograms were complicated by noise or another intervening event, few of the P-phase picks were modified. The S-phase picks, however, were often shifted by as much as a few tenths of a second or were added if S had not been read previously. The difficulty with picking the S phases was due to the waveform complexity of many of these phases and to the fact that the data were read from vertical-component stations only. Correlations of waveforms among different seismograms allowed S phases to be picked with a greater degree of consistency. Earthquakes that did not belong to any family were compared with other earthquakes that had a similar arrival time pattern to insure that the S phases were being interpreted in a consistent manner.

Comparison between the distributions of these earthquakes before and after retiming (Fig. 9) provides some insight into the precision of the locations. The largest shift in location was 2.2 km vertically and 0.9 km horizontally. The standard deviations of the shifts were 0.25 km in the east-west direction, 0.14 km in the north-south direction, and 0.56 km in the vertical direction. After relocation most of the earthquakes were fo-

cussed within six tight hypocentral clusters, each of which represents virtually a point source. Hypocenters in a given cluster still scatter by up to 0.2 km laterally and 0.3 km vertically from the center of the cluster. Each of the five waveform families located below 4 km depth is spatially distinct from the others, while the five shallow waveform families have substantial overlap. The absolute location accuracy for the distribution of VT earthquakes is difficult to assess. There is considerable uncertainty in the parameters of the velocity model, even though these parameters were selected by trial and error to minimize the RMS residual between observed and computed arrival times. A change in the model parameters would change the relative locations of nearby earthquakes very little, but could shift and distort the current distribution somewhat, particularly through changing depths. To test the sensitivity of the locations to changes in the velocity model, we increased all the velocities by 1% and then relocated the same 57 volcano-tectonic earthquakes. Although the average RMS residual increased by just 0.002 s, the hypocenters were shifted upward by as much as 0.3 km. The average upward shift was 0.16 km, and no earthquake moved deeper. Horizontal displacements were much smaller, the largest being 0.083 km and the average, irrespective of direction, being 0.040 km.

In another test, we raised the velocity in the third layer, which was only weakly constrained by the VT data, from 6.4 to 6.8 km/s. This caused the average RMS residual to increase by about 50%, from 0.035 to 0.052 s. Again, all hypocenters were shifted upward and the maximum and average upward shifts were 1.82 km and 0.98 km, respectively. Horizontal shifts did not exceed 0.55 km and averaged 0.25 km irrespective of direction. A firm limit on the total bias that may be present in these locations is difficult to obtain, given our use of a horizontally layered model in a region that could have large lateral velocity variations. However, the sensitivity tests above, coupled with the good fit of the data to the selected velocity model and buttressed by our ability to correctly locate the crater shot, lead us to believe that the bias is less than about 0.15 km

7. VT earthquake locations

We investigated the scatter in the distribution of volcano-tectonic earthquakes resulting from phase-picking errors by carefully analyzing the arrivals of 57 earthquakes, including 23 earthquakes from December 15-16 when most were shallower than 3 km depth, and 34 earthquakes from December 27 when most were deeper than 3 km. For each earthquake a record section was plotted showing the RDN, NCT, RED, and RDT traces with a time resolution of 0.01 s. Using a light table to overlay and compare events, we found 36 earthquakes belonged to one of 10 families defined by nearly identical waveforms and arrival times. By comparing earthquakes within each family, we were able to uniformly pick P phases at all four stations and S phases at all stations but RDN. As mentioned earlier the RDN response was anomalous much of the time, preventing reliable identification of the S phase at this station. With the exception of a small number of cases, in most of which the seismograms were complicated by noise or another intervening event, few of the P-phase picks were modified. The S-phase picks, however, were often shifted by as much as a few tenths of a second or were added if S had not been read previously. The difficulty with picking the S phases was due to the waveform complexity of many of these phases and to the fact that the data were read from vertical-component stations only. Correlations of waveforms among different seismograms allowed S phases to be picked with a greater degree of consistency. Earthquakes that did not belong to any family were compared with other earthquakes that had a similar arrival time pattern to insure that the S phases were being interpreted in a consistent manner.

Comparison between the distributions of these earthquakes before and after retiming (Fig. 9) provides some insight into the precision of the locations. The largest shift in location was 2.2 km vertically and 0.9 km horizontally. The standard deviations of the shifts were 0.25 km in the east-west direction, 0.14 km in the north-south direction, and 0.56 km in the vertical direction. After relocation most of the earthquakes were fo-

cusssed within six tight hypocentral clusters, each of which represents virtually a point source. Hypocenters in a given cluster still scatter by up to 0.2 km laterally and 0.3 km vertically from the center of the cluster. Each of the five waveform families located below 4 km depth is spatially distinct from the others, while the five shallow waveform families have substantial overlap. The absolute location accuracy for the distribution of VT earthquakes is difficult to assess. There is considerable uncertainty in the parameters of the velocity model, even though these parameters were selected by trial and error to minimize the RMS residual between observed and computed arrival times. A change in the model parameters would change the relative locations of nearby earthquakes very little, but could shift and distort the current distribution somewhat, particularly through changing depths. To test the sensitivity of the locations to changes in the velocity model, we increased all the velocities by 1% and then relocated the same 57 volcano-tectonic earthquakes. Although the average RMS residual increased by just 0.002 s, the hypocenters were shifted upward by as much as 0.3 km. The average upward shift was 0.16 km, and no earthquake moved deeper. Horizontal displacements were much smaller, the largest being 0.083 km and the average, irrespective of direction, being 0.040 km.

In another test, we raised the velocity in the third layer, which was only weakly constrained by the VT data, from 6.4 to 6.8 km/s. This caused the average RMS residual to increase by about 50%, from 0.035 to 0.052 s. Again, all hypocenters were shifted upward and the maximum and average upward shifts were 1.82 km and 0.98 km, respectively. Horizontal shifts did not exceed 0.55 km and averaged 0.25 km irrespective of direction. A firm limit on the total bias that may be present in these locations is difficult to obtain, given our use of a horizontally layered model in a region that could have large lateral velocity variations. However, the sensitivity tests above, coupled with the good fit of the data to the selected velocity model and buttressed by our ability to correctly locate the crater shot, lead us to believe that the bias is less than about 0.15 km

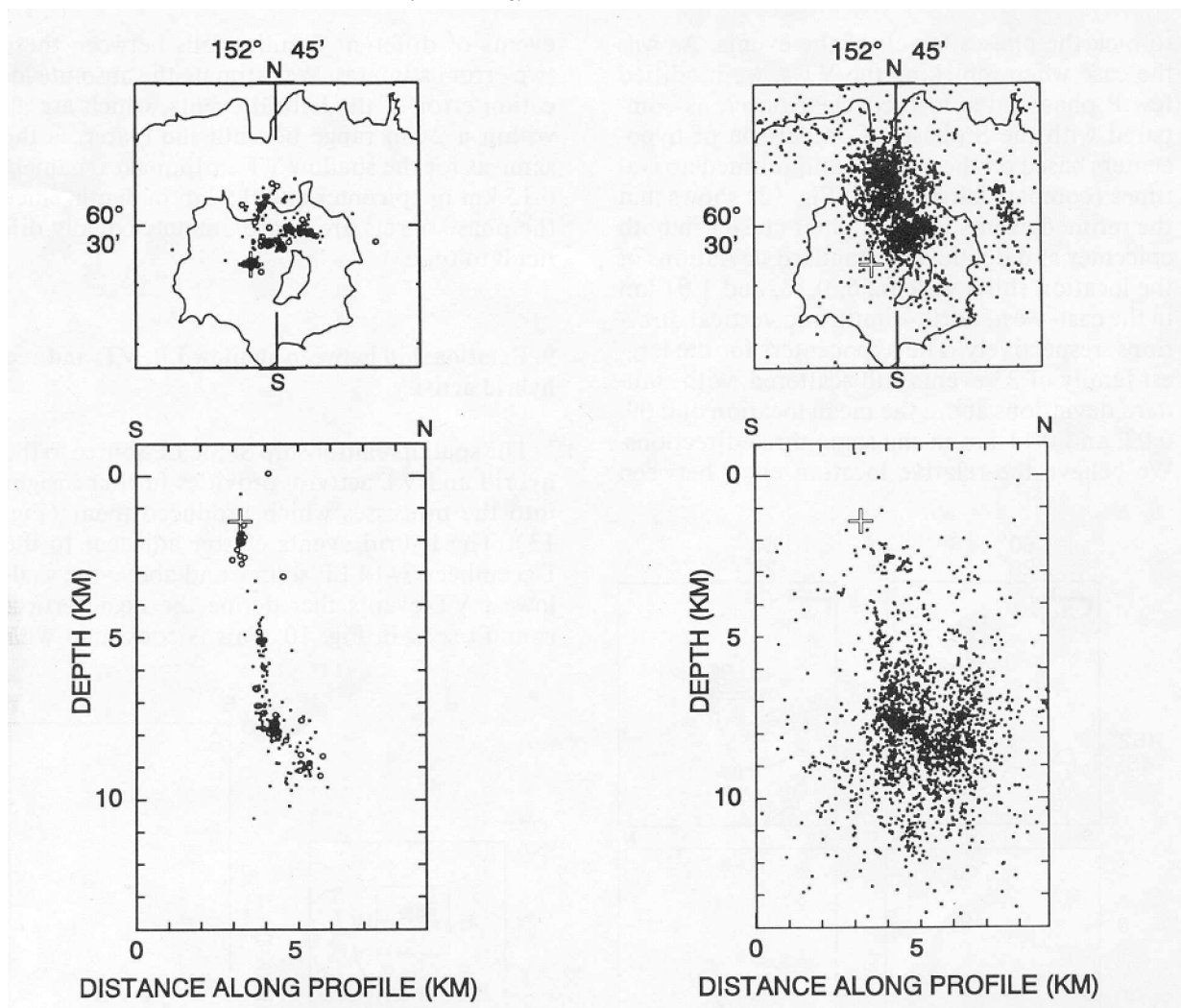


Fig. 10. Map (upper) and north-south vertical section at same scale (lower) of the VT earthquake hypocenters from December 14, 1989-January 2, 1990, including both relocated (circles) and unrelocated (dots) hypocenters. Cross indicates location of initial LP swarm.

Fig. 11. Map (upper) and north-south vertical cross section at same scale (lower) views of the VT earthquake hypocenters from January 3-December 31, 1990. Cross indicates location of initial LP swarm.

activity reflects the relaxation of the region surrounding a plexus of dikes and/ or sills from which magma was withdrawn. Based on our error estimates for the VT earthquakes, precise re- location of all of the earthquakes would reduce the number of outliers apparent in Fig. II, and might resolve more details of the spatial structure of the 1990 activity, but would not markedly change the gross features of the seismicity presented here.

8. Hybrid event locations

To examine the source region of the hybrid events, we plotted a seismogram with a time resolution of 0.01 s from station RED for each of the 40 located hybrid events. By overlaying pairs of events, we found that all but seven belonged to one of four families displaying nearly identical waveforms, and that one family included more than half of the events. We took advantage of the waveform similarities from event to event

to pick the phases for all of the events. As was the case when repicking the VT's, we modified few p phases, due to their clear onset, as compared with the S phases. Comparison of hypocenters based on the original and retimed arrival times (compare left and right Fig. 12) shows that the retimed events form a tighter cluster in both epicenter and depth. The standard deviations of the location shifts were 0.56, 0.13, and 1.01 km in the east-west, north-south, and vertical directions, respectively. The hypocenters for the largest family of 23 events still scattered, with standard deviations about the mean location of 0.09; 0.02, and 0.11 km in the same three directions. We believe the relative location error between

events of different families falls between these two error estimates. We estimate the absolute location error of the hybrid events, which are all within a 2-km range beneath the crater, is the same as for the shallow VT earthquakes, namely 0.15 km in epicenter and 0.5 km in depth, since the phase onsets are approximately equally difficult to time.

9. Relationship between shallow LP, VT, and hybrid activity

The spatial relationship of the LP source to the hybrid and VT activity provides further insight into the processes which produced them (Fig. 13). The hybrid events cluster adjacent to the December 13-14 LP source and above the shallowest VT events that define the near-vertical conduit seen in Fig. 10. This is consistent with

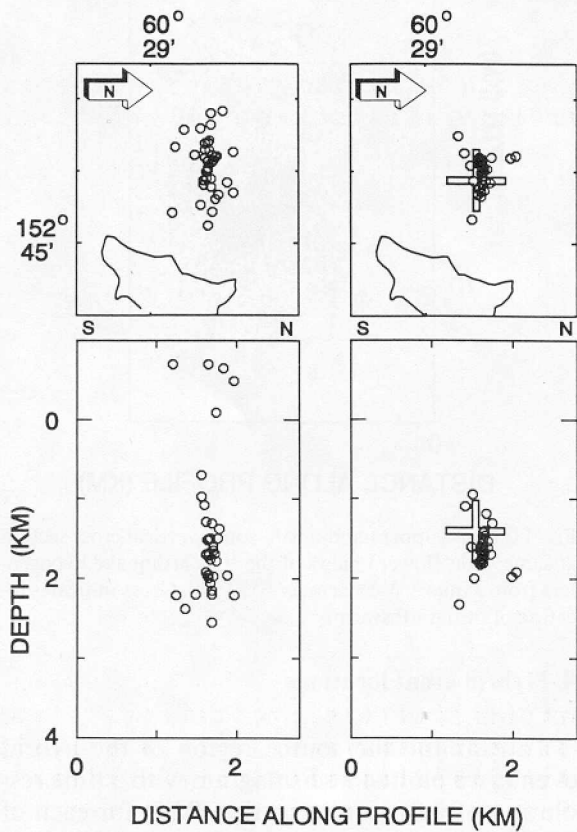


Fig. 12. Comparison of hypocenters of hybrid events from December 14, 1989 to January 2, 1990, based on original (left) and repicked (right) phase arrival times. Upper: map view, rotated so that north is to the right. Lower: north-south vertical section at same scale. Cross indicates location of initial LP swarm.

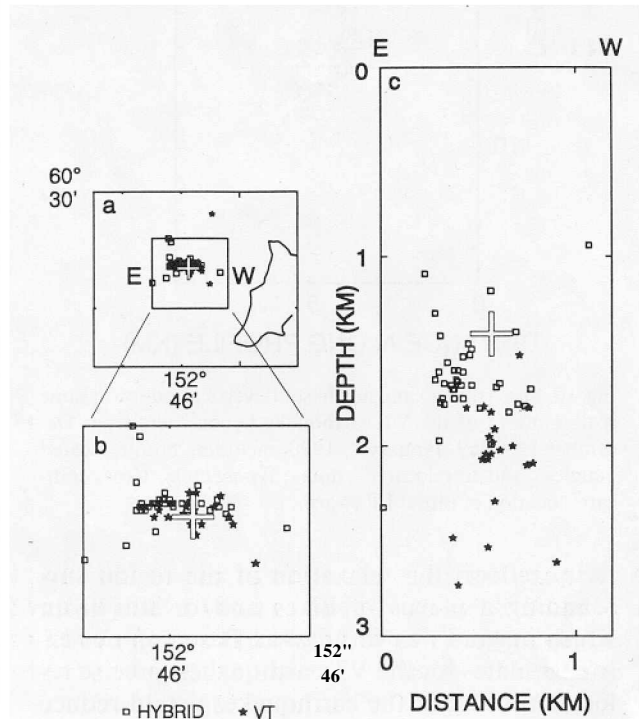


Fig. 13. Comparison of hypocenters of hybrid (squares) and volcano-tectonic (stars) events shallower than 3 km depth with source of initial LP swarm (cross). Inner square in (a) indicates region expanded in map (b) and vertical east-west section (c) at same scale as expanded map.

our inference that the hybrid events were due to brittle failure, either shear or tensile, in a zone intersecting a fluid-filled crack. The question arises whether the 0.4 km east-west elongation of the hybrid zone reflects the extent of the fracture zone or simply results from the poorer epicentral control in this direction, as noted above. No single hybrid family spanned the entire width, and the relative bias between families is difficult to assess, because the S-phase waveforms differ, and a different interpretation of where to pick the S-phase arrival might shift the epicenter. To eliminate the S-phase arrivals as a source of bias, the hybrid events were relocated without using the S phases. This increased the east-west separation between families even more, so we conclude that the true distribution is extended in this direction and reflects the strike of the fracture system on which the hybrid events occurred. The true east-west extent is estimated to be at least 0.2 km but not more than 0.4 km.

10. Magnitude distributions

Computed magnitudes for events of the 1989-1990 Redoubt sequence, which were only determined for the subset of events that could be located, range from M -0.9 to 2.2. The magnitude distributions for the three event types are summarized in Fig. 14. The VT magnitudes larger than M 0.4 follow the Gutenberg-Richter distribution, with the number of events decreasing by about a factor of 10 for each unit increase in magnitude. This distribution is typical of after-shock sequences and normal earthquake activity. Due to the limited detection sensitivity of the network to smaller events, the VT distribution deviates from this distribution below M 0.4. The magnitudes for the LP swarm of December 13-14 does not have the same distribution shape. There is an abrupt cutoff above M 1.4, and the number of events per interval is nearly uniform between M 0.4 and M 1.4. The December 26-January 2 LP swarm appears to have a peaked distribution near M 0.3 which likewise does not fit a Gutenberg-Richter distribution. This peaked character, however, may be an artifact of

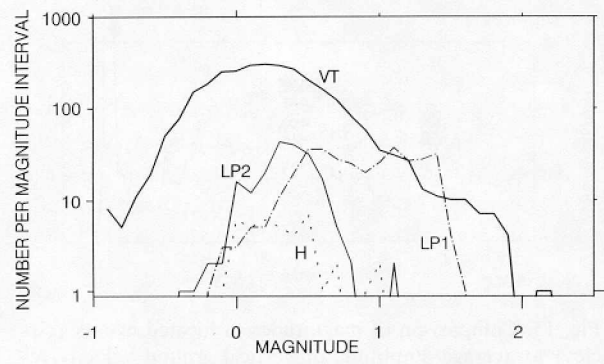


Fig. 14. Magnitude distribution for various event types. The logarithm of the number of events of a given magnitude, where magnitude is rounded to the nearest tenth, is plotted versus magnitude for VT earthquakes of December 1989-December 1990, LP events in the initial swarm of December 13-14 (*LP1*), LP events in the swarm of December 27, 1989-January 2, 1990 (*LP2*), and hybrid events of December 13, 1989, -January 2, 1990 (*H*).

the detection limitations of the network. subsequent swarms were clear only on SSAM and helicorder records and some were only recognized in hindsight (Stephens et al., 1994-this volume). These later events seldom triggered the *MDETECT* system; and when they were captured, too few phases could be read to allow a location and magnitude to be computed. By comparison with the earlier swarms, the magnitudes of the events in the later swarms must have been less than about M 0. The magnitude range of hybrid events is -0.2 to 1.0, similar to that of the second LP swarm, but there are too few events to determine if the size distribution is more similar to that of the VT earthquakes or the LP events.

The time sequence of magnitudes for the December 13-14 LP swarm shows a steady increase in the size of the largest events up until 21:00 AST on December 13 and then a steady decline throughout the remainder of the swarm (Fig. 15). Throughout the swarm, the rate of LP activity continued to increase, but the number of located events declines beginning near 22:00 on December 13 due to desensitization of the event-recording system by elevated long-term-average signal levels and the decrease in the magnitudes of the larger LP events. The Real-Time Seismic Amplitude Measurement (RSAM) system com-

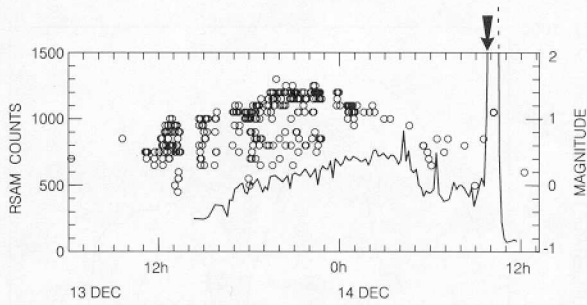


Fig. 15. Comparison of magnitudes of located events (circles) to average amplitude of vertical ground velocity recorded at station RDN (heavy line) during LP event swarm of December 13-14, 1989. Amplitudes are expressed in RSAM counts (see text) and were computed from data continuously recorded on a Masscomp computer system and corrected for automatic gain-ranging (Stephens et al., 1994-this volume). During the initial eruption, which began at 09:47 on December 14 (arrow along top margin), the RSAM amplitude reached 4987 counts, which exceeds the scale of this figure.

puts 10-min averages of the absolute amplitude of ground velocity and thus permits the radiated seismic energy to be monitored even when event-detection systems become desensitized (Endo and Murray, 1991). The total radiated seismic energy, as reflected in the RSAM record from RDN, shows a steady increase followed by a decrease. The amplitude pattern is generally consistent with the increasing and decreasing magnitude trends of the located events but the decrease in RSAM amplitude begins about 03:30 AST on December 14, 6.5 hours later than the peak in magnitudes. Between 21:00 AST on December 13 and 03:30 AST on December 14 the increasing rate of events more than compensates for the declining magnitudes so that the total radiated energy continues to increase. By the end of the swarm, the small LP events are occurring so frequently as to overlap one another and to constitute continuous tremor. A comparable evolution from discrete LP events that increased and then decreased in magnitude, and eventually merged into continuous tremor, was observed at Kilauea volcano, Hawaii, in 1981 in association with a rift intrusion (see fig. 45.13, Koyanagi et al., 1987). This similarity suggests that the underlying physical process may be similar at both locations.

II. Discussion

This paper summarizes the results of our classification and location of seismic events associated with the 1989-1990 eruption of Redoubt Volcano. The LP events and VT earthquakes have distinct locations, seismic signatures, and magnitude distributions. The former appear to originate from point sources, are dominated by energetic extended quasi-monochromatic coda, and are characterized by a rectangular magnitude distribution. The latter represent a broad spatial distribution of sources, are characterized by distinct broadband high-amplitude P- and S phases, and show a typical Gutenberg-Richter magnitude distribution. We believe the LP events result from the volumetric excitation of fluid-filled cracks or conduits involved in the upward transport of a mixture of water with steam and/or other magmatic gases (Chouet et al., 1994-this volume), while the VT earthquakes involve brittle failure of rock. In the 6-10 km depth range VT's may primarily reflect stress perturbations associated with the evacuation of magma, whereas at shallower depths they define a conduit structure and reflect stress changes associated with the injection and transport of magma and volatiles to the surface.

The use of both spectrograms and seismograms was found to be very helpful for properly classifying events. By treating the LP and VT events separately and by carefully reviewing waveforms and arrival-time statistics, we found that the distributions of LP events for the swarms of December 13-14 and December 27-January 2 cannot be distinguished from point sources 1.0 km apart. In contrast to the apparent cylindrical distribution of LP events, which are interpreted as an artifact, the apparent pipe-like distribution of VT earthquakes was found to be a true feature of the seismicity and could not be explained by either bias or scatter in the locations. The location of the hybrid events in a zone just beneath the LP source and just above the shallowest VT earthquakes is consistent with a mechanism for the hybrid events that involves both brittle failure and excitation of a fluid-filled crack. The hybrid events, which can be located more easily

than LP events due to their more impulsive onsets, may provide the best clue to the dimensions of the LP source. Precise relative relocations of the hybrid events are consistent with an east-west-oriented LP source zone that is narrow in the north-south direction but 0.2-0.4 km wide in the east-west direction. This width is close to the crack scale length of 0.14-0.38 km estimated by Chouet et al. (1994-this volume) in modeling the LP events in the December 13-14 swarm.

Acknowledgements

We acknowledge the valuable help of many participants in the Alaska Volcano Observatory, both for help in the 24-hour monitoring effort during December 1989 through May 1990 and for valuable discussions. In particular we thank John Davies for providing continuously recorded digital data from RDN; Tom Murray, John Rogers and Willie Lee for programming and technical support; and Gail March for much needed assistance in keeping the data recording system operational and for streamlining many of the routine data-processing tasks. Phil Dawson and Mahadeva Iyer provided thorough and helpful reviews.

References

- Aki, K., Fehler, M. and Das, S., 1977. Source mechanism of volcanic tremor: Fluid-driven crack models and their application to the 1963 Kilauea eruption. *J. Volcanol. Geotherm. Res.*, 2: 259-287.
- Chouet, B., 1985. Excitation of a buried magmatic pipe: A seismic source model for volcanic tremor. *J. Geophys. Res.*, 90: 1881-1893.
- Chouet, B., 1988. Resonance of a fluid-driven crack: Radiation properties and implications for the source of long-period events and harmonic tremor. *J. Geophys. Res.*, 93: 4373-4400.
- Chouet, B., 1992. A seismic model for the source of long period events and harmonic tremor. In: P. Gasparini, R. Scarpa and K. Aki (Editors), *Volcanic Seismology*. IAV-CEI Proc. in Volcanology, Springer-Verlag, Berlin, 3: 133-156.
- Chouet, B.A., Page, R.A., Stephens, C.D., Lahr, J.C. and Power, J.A., 1994. Precursory swarms of long-period events at Redoubt Volcano (1989-1990), Alaska: Their origin and use as a forecasting tool. In: T.P. Miller and B.A. Chouet (Editors), *The 1989-1990 Eruptions of Redoubt Volcano, Alaska*. *J. Volcanol. Geotherm. Res.*, 62: 95-135.
- Dawson, P. B., Chouet, B.A., Page, R.A. and Lahr, J.C., 1992. A post-eruptive seismic survey of Redoubt Volcano, Alaska. *Seismol. Res. Lett.*, 63: 67.
- Endo, E.T. and Murray, T., 1991. Real-time Seismic Amplitude Measurement (RSAM): A volcano monitoring and prediction tool. *Bull. Volcanol.*, 53: 533-545.
- Klein, F. W., 1978. Hypocenter location program HYPOIN-VERSE; Part I: Users guide to Versions 1, 2, 3, and 4, U.S. Geol. Surv., Open-File Rep. 78-649, 113 pp.
- Koyanagi, R. Y., Chouet, B. and Aki, K., 1987. Origin of volcanic tremor in Hawaii, Part I, Data from the Hawaiian Volcano Observatory 1969-1985. In: R.W. Decker, T.L. Wright and P.H. Stauffer (Editors), *Volcanism in Hawaii*. U.S. Geol. Surv., Prof. Pap., 1350: 1221-1257.
- Lee, W.H.K. and Lahr, J.C., 1975. HYPO71 (Revised): A computer program for determining hypocenter, magnitude, and first motion pattern of local earthquakes. U.S. Geol. Surv., Open-File Rep., 75-311, 113 pp.
- Lahr, J.C., 1989. HYPOELLIPSE/Version 2.0: A computer program for determining local earthquake hypocentral parameters, magnitude, and first motion pattern. U.S. Geol. Surv., Open-File Rep. 89-116, 92 pp.
- Lienert, B.R., Berg, E. and Frazer, L.N., 1986. HYPOCENTER: An earthquake location method using centered, scaled, and adaptively damped least squares. *Bull. Seismol. Soc. Am.*, 76: 771-783.
- Power, J.A., Lahr, J.C., Page, R.A., Chouet, B.A., Stephens, C.D., Harlow, D.H., Murray, T.L. and Davies, J.N., 1994. Seismic evolution of the 1989-1990 eruption sequence of Redoubt Volcano, Alaska. In: T.P. Miller and B.A. Chouet (Editors), *The 1989-1990 Eruptions of Redoubt Volcano, Alaska*. *J. Volcanol. Geotherm. Res.*, 62: 69-94.
- Stephens, C.D., Chouet, B.A., Page, R.A., Lahr, J.C. and Power, J.A., 1994. Seismological aspects of the 1989-1990 eruptions at Redoubt Volcano, Alaska: The SSAM perspective. In: T.P. Miller and B.A. Chouet (Editors), *The 1989-1990 Eruptions of Redoubt Volcano, Alaska*. *J. Volcanol. Geotherm. Res.*, 62: 153-182.
- Tottingham, D.M., Lee, W.H.K. and Rogers, J.A., 1989. User manual for MDETECT. In: W.H.K. Lee (Editor), *Tool-box for Seismic Data Acquisition, Processing and Analysis*. International Association of Seismology and Physics of the Earth's Interior.